processes

MDPI

*Article*

# Resonance Suppression Method Based on Hybrid Damping Linear Active Disturbance Rejection Control for Multi-Parallel Converters

**Minhui Qian [1,2], Baifu Zhang [1,*], Jiansheng Zhang [1], Wenping Qin [1], Ning Chen [2] and Yanzhang Liu [2]**

[1] Electrical and Power Engineering, Taiyuan University of Technology, Taiyuan 030024, China; minhui_qian@163.com (M.Q.); zhang-jsh@tsinghua.edu.cn (J.Z.); qinwenping@tyut.edu.cn (W.Q.)
[2] National Key Laboratory of Renewable Energy Grid-Integration, China Electric Power Research Institute, Beijing 100192, China; chenning8375@163.com (N.C.); lyz4534@163.com (Y.L.)
* Correspondence: zhangbaifu92@126.com; Tel.: +86-182-3412-6802

**Abstract:** The parallel operation of multiple LCL-type converters will result in a deviation of the resonant frequency and resonance phenomena. The occurrence of harmonic resonance can cause problems such as an increase in harmonic voltage and current. This can lead to the malfunction of relay protection and automatic devices, causing damage to system equipment. In severe cases, it can cause accidents and threaten the safe operation of the power system. A hybrid damping active disturbance rejection control (HD-ADRC) method is proposed in this paper to suppress the harmonic resonance of parallel LCL-type converters. First, a third-order linear disturbance rejection controller (LADRC) including the linear extended-state observer and the error-feedback control rate is designed based on LCL-type converter model analysis. The proposed method considers the resonance couplings caused by both internal and external disturbances as the total disturbance, thus improving the anti-disturbance capabilities as well as the operational stability of converters in parallel. Then, a hybrid damping control is proposed to reconstruct the damping characteristics of converters to suppress the parallel resonance spike and reduce the resonance frequency offset. And the parameter selection of the control system is optimized through a stability analysis of the tracking performance and anti-disturbance performance of the HD-ADRC controller. Finally, all the theoretical considerations are verified by simulation and experimental results based on the Matlab/Simulink 2018B and dSpace platform. The simulation and experimental results show that the PI controller gives a THD of 5.33%, which is reduced to 4.66% by employing the HD-LADRC, indicating an improved decoupling between the converters working in parallel with the proposed control scheme.

**Keywords:** hybrid damping active disturbance rejection control; linear active disturbance rejection controller; LCL-type converter; resonance suppression



**Citation:** Qian, M.; Zhang, B.; Zhang, J.; Qin, W.; Chen, N.; Liu, Y. Resonance Suppression Method Based on Hybrid Damping Linear Active Disturbance Rejection Control for Multi-Parallel Converters. *Processes* **2024**, *12*, 2152. https://doi.org/10.3390/pr12102152

Academic Editor: Hsin-Jang Shieh

Received: 27 August 2024
Revised: 24 September 2024
Accepted: 29 September 2024
Published: 2 October 2024



## 1. Introduction

As a representative of distributed generation (DG), PV power can be consumed at or near the user site, which reduces the line loss of long-distance transmission, improves voltage distribution, and increases the operational reliability of the distribution system [1–4]. However, power electronic converters are always required as an interface between PV and the utility grid. Most grid-connected converters employ the conventional three-phase full-bridge topology, where the switching behavior of the semiconductor devices generates harmonics. To address the issue, relevant standards are formulated to ensure a stringent regulation of supply quality. One of the effective harmonic suppression methods is to add passive filter networks on the output side of the grid-tied converters, such as L-type filters, LCL filters, and other improved filter networks [5–7].

Compared to L-type filters, an LCL-type filter needs smaller filter inductance and thus a reduced size. Also, it provides better attenuation of high-frequency harmonic

currents, limits the inrush current in the filter capacitor, and increases the robustness of the converter [8]. However, the risk of resonance brought by its third-order characteristic is the biggest safety hazard [9,10]. Furthermore, the operations of parallel converters are affected by a variety of factors, such as the grid impedance, hardware parameters, and the number of operating converters, all contributing to possible resonance among parallel converters [11–13].

Both passive and active damping methods have been proposed to suppress the resonance caused by LCL-type filters [14,15]. Passive damping directly improves the damping characteristics by adding passive components to the filter network [16]. However, the extra passive devices add to the circuit complexity and bring up filter size, costs, and system loss, which limit its use in practice. To address these shortcomings, active damping is proposed, and it can be broadly classified into three categories: single-loop control [8], multi-loop control [17], and complex control [18]. Unlike passive damping to add actual components, active damping employs a virtual damping form to the feedback control loop to avoid aforementioned drawbacks while still achieving adequate damping characteristics. In the literature, Ref. [19] proposed a phase lead compensator to compensate system phase margin in the Vpcc feedback loop, which will decrease the phase shift of the resonance frequency. A hybrid active damping method is studied in [20] to suppress the resonance peak value, which combines the capacitor-current-feedback and unit PCC voltage feedforward. For an LCL-equipped high-speed permanent magnet synchronous motor, a flexible active damping method is proposed in [21]. In the paper, the damping ratio of the LCL resonance can be freely designed using the proposed high-order partial-state (virtual output voltage and the capacitor current) feedback. In [22], the resonance characteristics of parallel systems are divided into two categories: static and dynamic resonance, and then a hybrid multi-resonance suppression method based on the improved dual-division-summation (D-D-Σ) method, and a virtual admittance strategy is proposed. An active disturbance rejection control (ADRC) control scheme is proposed in [23] for the LCL-type grid-connected inverter. With the proposed strategy, only the grid-injected current is sensed to achieve the objectives of grid-injected current direct control and robust resonance damping for the LCL-type grid-connected inverter. The shunt capacitor harmonic voltage is regulated in [24] according to a term that is associated with both the harmonic load current and the HAPF harmonic line current. In [25], only the resonance mechanism and characteristics of a real large-scale PV plant are explored, and the practical case of harmonic resonance in the studied PV plant is investigated. The voltage transmission equations are derived in [26] to analyze the transmission characteristics of harmonic voltages along a long feeder. And a new control strategy for inverters is proposed to suppress the multiple resonances in current and the amplification of harmonic voltages. The authors of [27] propose a general stability control concept for power converters from the view of the impedance magnitude. However, the active damping relies on the accuracy of the components' parameters, which varies gradually due to the environment and other factors. This shifts the resonance point and eventually has a negative impact on the robustness of the control.

The active disturbance rejection control (ADRC) balances the overshoot and response speed to improve the robustness of the converter. The authors of [28] proposed a linearization method for ADRC (LADRC) to reduce the complexity of parameter tuning by classifying the control parameters into controller bandwidth and observer bandwidth without affecting the controller performance. In essence, the LADRC introduces an expansive state observer that estimates and compensates for disturbances. In [29], an adaptive LADRC is proposed to facilitate parameter tuning of the controller and realize the real-time self-adaptive optimization of parameters. A LADRC is applied to PLL in [30], and the system stabilities of the grid-connected inverters with LADRC-PLL and PI-PLL are compared. The grid-connected inverter with LADRC-PLL has better adaptability to the weak grid and demonstrates a certain ability to suppress the sub- and super- synchronous oscillation. A modified linear extended-state observer is designed in [31] to estimate the value and differential value of total disturbance, significantly reducing the estimated error.

In [32], a robust active damping method based on LADRC is proposed for PWM converters, and the Padé approximation is used to reduce the order of the controlled object transfer function. This improves the power quality and dynamic performance in the presence of parameter uncertainty and external disturbances. A LADRC control strategy is proposed for a three-phase voltage-based PWM rectifier in [33]. A linear extended-state observer is used to observe and compensate the coupling variables and external disturbances in the PWM rectifier model in two identical step coordinate systems. In order to reduce the capacity of the active power filter and improve its dynamic tracking speed and anti-interference capability for harmonic currents, a fuzzy LADRC for the external voltage loop control of the injected hybrid power filter is proposed in [34]. The introduced fuzzy control solves the difficult problem of controller parameter rectification and proves the stability of the system using the Lyapunov stability definition. However, only the control system's coupling and the immunity of the converter are studied in the above studies. So far, the interactive coupling and resonance characteristics among multiple LCL-type converters have yet to be considered.

In this paper, an HD-ADRC method is proposed to suppress the harmonic resonance of parallel LCL-type converters, where both the internal and external disturbances are lumped together as total disturbances.

The contribution of this paper is summarized as follows:

(1) A third-order linear disturbance rejection controller (LADRC) with a linear extended-state observer and an error feedback control rate is designed based on LCL-type converter model analysis.
(2) A hybrid damping control is proposed to reconstruct the damping characteristics of converters to suppress the parallel resonance spike and to reduce the resonance frequency offset.
(3) The parameter selection of the control system is optimized through the stability analysis of tracking performance and anti-disturbance performance of the HD-ADRC controller.

## 2. Analysis of Fault Propagation Mechanism in DC Sub-Grid Coupling Characteristics Analysis of Parallel LCL-Type Converter

### *2.1. Modeling of the LCL-Type Converter*

The topology of the LCL-type converter is shown in Figure 1. Ideal conditions are assumed to facilitate the converter modeling. According to Kirchhoff's law, the filter is described in the time domain as [35]:

$$\begin{cases} \frac{di_{1k}}{dt} = -\frac{1}{L_1}u_{ck} + \frac{1}{L_1}u_{1k} \\ \frac{du_{ck}}{dt} = \frac{1}{c}i_{1k} - \frac{1}{c}i_{2k} \\ \frac{di_{2k}}{dt} = \frac{1}{L_2}u_{ck} - \frac{1}{L_2}u_{pcc} \end{cases} \quad k = a, b, c \tag{1}$$

where, $i_{1k}$ is the converter side current, $u_{ck}$ is filter capacitor voltage, $i_{2k}$ is the grid side current, $u_{1k}$ is the converter output voltage, and $u_{pcc}$ is the voltage of PCC. Transform (1) to $dq0$:

$$\begin{cases} \frac{di_{1d}}{dt} = \omega i_{1q} - \frac{1}{L_1}u_{cd} + \frac{1}{L_1}u_{1d} \\ \frac{di_{1q}}{dt} = -\omega i_{1d} - \frac{1}{L_1}u_{cq} + \frac{1}{L_1}u_{1q} \\ \frac{du_{cd}}{dt} = \frac{1}{C}i_{1d} - \frac{1}{C}i_{2d} + \omega u_{cq} \\ \frac{du_{cq}}{dt} = \frac{1}{C}i_{1q} - \frac{1}{C}i_{2q} - \omega u_{cd} \\ \frac{di_{2d}}{dt} = \omega i_{2q} + \frac{1}{L_2}u_{cd} - \frac{1}{L_2}u_{dpcc} \\ \frac{di_{2q}}{dt} = -\omega i_{2d} + \frac{1}{L_2}u_{cq} - \frac{1}{L_2}u_{qpcc} \end{cases} \tag{2}$$

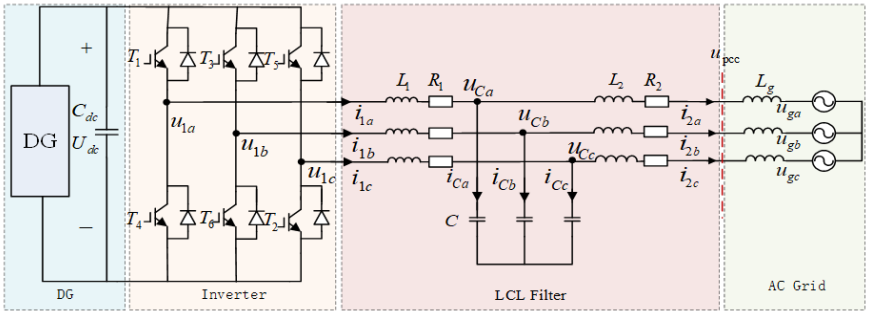


**Figure 1.** Topology of the LCL-type converter.

As suggested in (2), the *dq* components of grid side current $i_{2k}$ are coupled, which affects the response time and control accuracy of the feedback control. In addition, the inherent third order of the LCL filter would exacerbate the coupling and thus control performance.

### *2.2. Modeling of Parallel LCL-Type Converters*

It is worth noting that the output current of a converter is affected not only by the grid impedance, but also other converters operating in parallel. In order to observe the coupling mechanism of paralleled converters, a single converter is first modeled in Figure 2, where the open-loop transfer function of the converter with its feedback control are written as follows [36]:

$$G_O(s) = G_i(s)G_{inv}(s)G_{LCL}(s) = \frac{G_i(s)G_{inv}(s)}{s^3L_1L_2C + s(L_1 + L_2)} \tag{3}$$

where $G_i(s)$ is the transfer function of the PI controller, $G_{LCL}(s)$ is the transfer function of the LCL filter, $G_{inv}(s)$ is the gain of the transform bridge including digital control delay. $G_{inv}(s)$ is expressed as:

$$G_{inv}(s) = \frac{u_{dc}}{(1.5T_s s + 1)} \tag{4}$$

where $u_{dc}$ is the DC voltage, and $T_s$ is the sampling period.

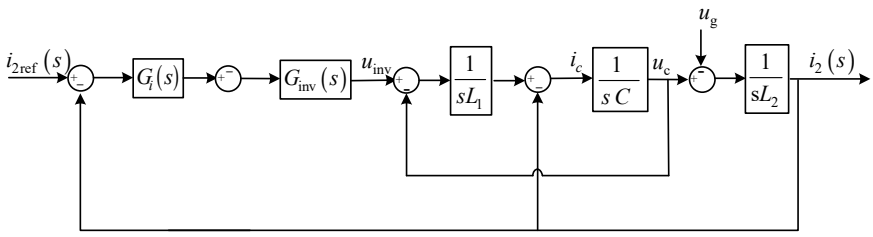

**Figure 2.** Control block of the LCL-type converter.

The output current of the converter is:

$$\begin{aligned} i_2(s) &= \frac{G_O(s)}{1+G_O(s)} i_{2ref}(s) - \frac{G_Y(s)}{1+G_O(s)} U_{PCC}(s) \begin{pmatrix} a_{11} & a_{12} & a_{13} \\ a_{21} & a_{22} & a_{23} \\ a_{31} & a_{32} & a_{33} \end{pmatrix} \\ &= G_t(s) i_{2\mathrm{ref}}(s) - Y_{eq}(s) U_{\mathrm{pcc}}(s) \end{aligned} \tag{5}$$

where Gt(s) is the Norton equivalent controlled-current source coefficient, Gt(s)i2ref(s) is the equivalent controlled-current source, and Yeq(s) is the equivalent output admittance of the converter.

$$\begin{cases} G_t(s) = \frac{G_i(s)G_{inv}(s)}{s^3L_1L_2C + s(L_1+L_2) + G_i(s)G_{inv}(s)} \\ Y_{eq}(s) = \frac{s^2L_1C+1}{s^3L_1L_2C + s(L_1+L_2) + G_i(s)G_{inv}(s)} \end{cases} \tag{6}$$

The Norton equivalent model of a converter and the utility grid is obtained from (6), where $Y_{eq}(s)$ is the equivalent admittance of the converter.

Ideally, if the grid impedance is neglected, the equivalent admittance of the converter can be corrected to cancel the pole of the right half plane to improve the stability of the system. However, in the presence of a weak grid, the grid impedance, coupled with aggregated converters, is often found to be the essential factor for harmonic resonances and stability problems. Now, the Norton model can be extended to a system of $n$ paralleled converters as shown in Figure 3, where $i$ is the $i$-th converter.

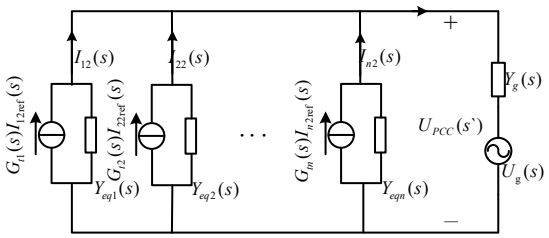


**Figure 3.** Norton equivalent circuit for multi-parallel converters.

According to Kirchhoff's law, the relationship between the controlled-current source and the voltage at PCC can be obtained as follows:

$$\sum_{j=1}^{n} G_{tj}(s)I_{j2ref}(s) - U_{PCC}(s)\sum_{j=1}^{n} Y_{eqj}(s) = Y_g(s)[U_{PCC}(s) - U_g(s)] \tag{7}$$

Substituting Formula (5) into (7), the output current of the i-th converter is obtained as follows:

$$I_{2i}(s) = F_i(s)I_{i2ref}(s) - \sum_{j=1,j\neq i}^{n} P_{jt}(s)I_{j2ref}(s) - S_i(s)U_g(s) \tag{8}$$

where

$$\begin{cases} F_i(s) = G_{ti}(s)\dfrac{(\sum_{j=1,j\neq i}^{n} Y_{eqj}(s)+Y_g(s))}{(\sum_{j=1}^{n} Y_{eqj}(s)+Y_g(s))} \\ P_{it}(s) = \dfrac{G_{ti}(s)Y_{eqj}(s)}{\sum_{j=1}^{n} Y_{eqj}(s) + Y_g(s)} \\ S_i(s) = \dfrac{Y_{eqi}(s)Y_g(s)}{\sum_{j=1}^{n} Y_{eqj}(s) + Y_g(s)} \end{cases} \tag{9}$$

In the parallel converters system, (8) gives a functional expression of the i-th converter output current. It is also clear that converters are coupled with the grid impedance to form a complex high-order coupling network. The essential factors affecting the output current of a converter include the reference current and the output reference current of other converters, as well as the grid voltage. When the grid impedance Zg is equal to 0 (Yg tends towards infinity), the output current of the converter is only linked to its own output reference current and becomes independent of other converters. When taking grid impedance Zg into consideration, the coupling between converters becomes an essential factor in causing harmonic resonances and instability.

## 3. Hybrid Damping-Linear Active Disturbance Rejection Control Framework

Putting the above essential factors causing coupling problems in perspective, a resonance suppression scheme based on Hybrid Damping-linear Active Disturbance Rejection Control (HD-LADRC) is proposed in this paper. Figure 4 shows HD-LADRC diagram for parallel LCL-type converters, which consists of a Linear Extended-State Observer (LESO), Linear-State Error Feedback (LSEF), differential feedforward compensation, and a hybrid damping controller [37–40].

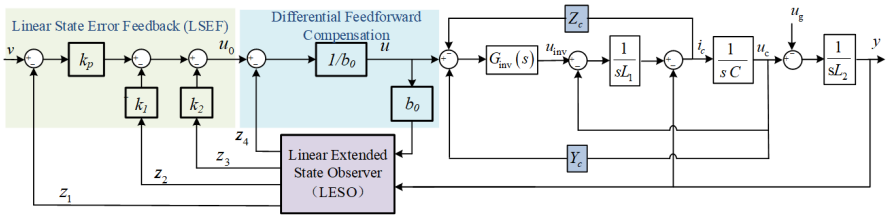


**Figure 4.** HD-LADRC diagram.

### *3.1. LADRC*

The third-order time domain model of the grid-connected current can be rewritten as the sum of the standard estimator and total disturbance. The expression is shown as:

$$\begin{cases} \frac{d^3 i_{2d}}{dt^3} = b_0 u_d + \Delta b u_d + f_{0d} + w_d = b_0 u_d + f_d \\ \frac{d^3 i_{2q}}{dt^3} = b_0 u_q + \Delta b u_q + f_{0q} + w_q = b_0 u_q + f_q \end{cases} \tag{10}$$

where $b_0 = 1/(L_1 C L_2)$ is the approximate estimation of the system control gain and $\Delta b$ is the system modeling error. $u_d$ and $u_d$ are the $dq$ axis components of the control system output, respectively. $f_{0d}$ and $f_{0q}$ are $dq$ axis components of internal disturbances including coupling components. $w_d$ and $w_q$ are $dq$ axis components of external disturbances, respectively. Since the LADRC lumps all the effects as disturbances, in the following analysis the $dq$ axis control variables are decoupled, and the lower subscript discrimination is not carried out.

The fourth-order linear extended-state observer is:

$$\begin{cases} \begin{bmatrix} \dot{Z}_1 \\ \dot{Z}_2 \\ \dot{Z}_3 \\ \dot{Z}_4 \end{bmatrix} = \underbrace{\begin{bmatrix} -\beta_1 & 1 & 0 & 0 \\ -\beta_2 & 0 & 1 & 0 \\ -\beta_3 & 0 & 0 & 1 \\ -\beta_4 & 0 & 0 & 0 \end{bmatrix}}_{A\text{-}LC} \begin{bmatrix} Z_1 \\ Z_2 \\ Z_3 \\ Z_4 \end{bmatrix} + \underbrace{\begin{bmatrix} 0 \\ 0 \\ b_0 \\ 0 \end{bmatrix}}_{B} u + \underbrace{\begin{bmatrix} \beta_1 \\ \beta_2 \\ \beta_3 \\ \beta_4 \end{bmatrix}}_{B} y \\ y = \underbrace{[1 \quad 0 \quad 0 \quad \cdots \quad 0]}_{c} Z \end{cases} \tag{11}$$

The system matrix **A-LC** is a Horwitz matrix. According to the bandwidth tuning method, the system matrix needs to be configured in the left half-plane of the system. In this case, the characteristic equation of the system is:

$$\lambda(s) = |sI - (A\text{-}LC)| = s^4 + \beta_1 s^3 + \beta_2 s^2 + \beta_1 s + \beta_4 = (s + \omega_0)^2 \tag{12}$$

where $\beta_1$, $\beta_2$, $\beta_3$, $\beta_4$, and $\omega_0$ are observer gains and bandwidth, respectively. The relationship between observer gain and bandwidth can be expressed as: $\beta_1 = 4\omega_0$, $\beta_2 = 6{\omega_0}^2$, $\beta_3 = 4{\omega_0}^3$, $\beta_4 = {\omega_0}^4$.

By selecting an appropriate observer bandwidth, the state matrix can be adjusted to have all the characteristic roots in the left half-plane. And the observed states $z_1$, $z_2$, $z_3$, and $z_4$ converge to the grid side current $I_2$, the first- and second-order differential, and the total disturbances, respectively, in such a way that the stability is maintained.

Based on the estimated system state variables and total disturbances, the output of the control system is designed as:

$$u = \frac{u_0 - Z_4}{b_0} \tag{13}$$

where $u_0$ is the proportional feedback controller of the system, which is expressed as:

$$u_0 = k_p(v - z_1) - k_1 z_2 - k_2 z_3 \tag{14}$$

where $k_p$, $k_1$, and $k_2$ are the controller gains. Considering the stability operation of the system, all the poles need to be placed at the controller bandwidth $\omega_c$. According to the parameter tuning method in [24], the relationship between the controller gain and the controller bandwidth can be obtained as follows: $k_p = {\omega_c}^3$, $k_1 = 3{\omega_c}^2$, $k_2 = 3\omega_c$.

It is noticed from (13) and (14) that LSEF consists of two parts: feedback control $u_0/b_0$ for fast dynamic response and disturbance compensation $-z_4/b_0$ to minimize the control error and to gain an improved anti-interference ability. Thus, the system can be equivalent to the integral series type.

$$\dddot{y} = b_0 u + f = b_0 \frac{u_0 - z_4}{b_0} + f = u_0 + (f - z_4) \approx u_0 \tag{15}$$

It is clearly demonstrated by (15) that (11)–(14) constitute the third-order LADRC for LCL-type converter.

### *3.2. Hybrid Damping Controller*

In the presence of weak grid, the number of paralleled units becomes an essential factor in terms of the resonance characteristic. As suggested in [23], the increase in the number of converters is equivalent to the increase in the grid impedance; that is, the parallel operation of $n$ converters is equivalent to the increase in the grid impedance by $n$ times, when the converters are operated in parallel. The LCL-type filter gain is written as:

$$G_{LCL}(s) = \frac{G_{inv}}{s^3 L_1(L_2 + nL_g)C + s(L_1 + L_2 + nL_g)} = \frac{G_{inv}}{sL_1(L_2 + nL_g)C} \frac{1}{s^2 + (2\pi f_r)^2} \tag{16}$$

where $n$ is the number of converters, and $L_g$ is the equivalent grid impedance. The resonant frequency can be rewritten as:

$$f_r = \frac{1}{2\pi} \sqrt{\frac{L_1 + L_2 + nL_g}{L_1(L_2 + nL_g)C}} \tag{17}$$

where $nL_g$ is the equivalent model when $n$ converters are connected in parallel. The change in the grid impedance $L_g$ has a greater impact on the resonance frequency, and the resonance frequency is a decreasing function of $L_g$.

In response to the above problems, this paper proposes the hybrid damping control strategy given in Figure 4, which simultaneously suppresses the resonant frequency offset and resonant spikes. The hybrid damping control method uses a combination of capacitance current feedback and capacitance voltage feedback control. According to Figure 4, the LCL-type filter gain can be derived as:

$$\begin{aligned} G_{LCL}(s) &= \frac{G_{inv}}{s^3 L_1(L_2+nL_g)C + s^2(L_2+nL_g)CG_{inv}Z_c + s[L_1+(L_2+nL_g)+(L_2+nL_g)G_{inv}Y_C]} \\ &= \frac{G_{inv}}{sL_1(L_2+nL_g)C(2\pi f_r)^2} \frac{(2\pi f_r)^2}{s^2 + s\frac{G_{inv}Z_c}{L_1} + (2\pi f_r)^2} \end{aligned} \tag{18}$$

where resonance frequency $f_r$ can be modified as:

$$f_r = \frac{1}{2\pi} \sqrt{\frac{L_1 + (L_2 + nL_g) + (L_2 + nL_g)G_{inv}Y_C}{L_1(L_2 + nL_g)C}} \tag{19}$$

According to (18), the LCL-type filter gain is equivalent to the product of the first-order system and the second-order oscillation system after hybrid damping control. The LCL-type filter gain has a pole at the origin and a pair of conjugate poles. Therefore, the capacitance current feedback coefficient and the capacitance voltage feedback coefficient can be adjusted through the second-order oscillation link. By reconstructing the damping characteristics of the system, the resonance frequency shift and resonance spikes can be suppressed.

The standard form of the second-order oscillation link is given by:

$$G(s) = \frac{(2\pi f_n)^2}{s^2 + 2\xi(2\pi f_n) + (2\pi f_n)^2} \tag{20}$$

where $\xi$ is the damping coefficient, and $f_n$ is the natural frequency of the system without damping. We then convert (20) to the complex frequency domain:

$$G(j\omega) = \frac{1}{1 - \frac{f^2}{f_n^2} + j2\xi\frac{f}{f_n}} \tag{21}$$

where the amplitude and phase expressions are given by:

$$\begin{cases} A(\omega) = \frac{1}{\sqrt{(1-\frac{f^2}{f_n^2})^2 + 4\xi^2\frac{f^2}{f_n^2}}} \\ \varphi(\omega) = -\arctan\frac{2\xi\frac{f}{f_n}}{1-\frac{f^2}{f_n^2}} \end{cases} \tag{22}$$

The minimum resonance peak point occurs when the damping coefficient is at 0.707. And the resonance frequency gradually increases and tends to the natural frequency without damping as the damping coefficient decreases. As the damping coefficient approaches 0, the system resonance peak reaches ∞, which corresponds to an undamped system. The damping coefficient is usually set to 0.707.

The capacitance current feedback impedance can be adjusted according to the second-order oscillation link:

$$Z_C = \frac{4\pi\xi L_1 f_r}{G_{inv}} \tag{23}$$

With the damping coefficient set to 0.707, the resonance peak can be calculated as:

$$\frac{d}{d\omega}\left[(1 - \frac{f^2}{f_n^2})^2 + 4\xi^2\frac{f^2}{f_n^2}\right] = 0 \tag{24}$$

The expression is derived as:

$$f_r = f_n\sqrt{1 - 2\xi^2} \tag{25}$$

Combining (19) and (25), the capacitance voltage feedback coefficient can be adjusted as:

$$Y_C = \frac{4\pi^2 f_n^2(1 - 2\xi^2)L_1(L_2 + nL_g)C - L_1 - (L_2 + nL_g)}{(L_2 + nL_g)G_{inv}} \tag{26}$$

To verify the harmonic resonance suppression effect, the Bode diagram of the LCL filter network is drawn in Figure 5 by substituting Formulas (23) and (26) and the parameters in Table 1 into Formula (18). Clearly, as the number of parallel converters increases from two to six, the resonance gain remains unchanged, but the resonance frequency shifts towards the lower frequency end. The red and green curves demonstrate approximately the same peak resonance suppression gain, while the proposed control has a reduced frequency offset, indicating a reduced probability of harmonic resonance in the paralleled setup. In summary, the hybrid damping control proposed in this paper has improved effects on the impedance reconstruction for the parallel converter system. It can effectively reduce the resonant frequency offset and suppress the resonant spike and therefore improves the impedance characteristics of the parallel converter system.

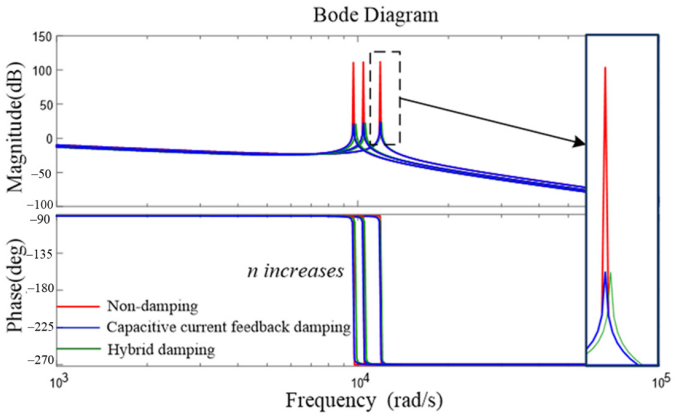


**Figure 5.** Comparison of resonance characteristics of LCL filter network.

**Table 1.** A Brief Description of the Literature.

| Ref. | Disturbance Model of LCL-Type Converter | Resonant Peak Suppression | Resonant Frequency Offset Suppression | Parallel Resonance Suppression |
|---|---|---|---|---|
| The proposed model | √ | √ | √ | √ |
| [14] | | √ | | |
| [15] | √ | √ | | |
| [16] | | √ | | |
| [8] | √ | √ | | |
| [17] | √ | √ | | |
| [19] | | | √ | |
| [20] | √ | √ | | |
| [21] | √ | √ | | |
| [22] | √ | √ | | √ |
| [23] | √ | √ | | |
| [24] | √ | √ | | |
| [25] | | √ | | |
| [26] | | √ | | |
| [27] | | √ | | |

## 4. Stability Analysis of LADRC

The Laplace transform of (11), (13), and (14) is performed as:

$$\begin{cases} sZ(s) = (A\text{-}LC)Z(s) + BU(s) + LY(s) \\ U(s) = \frac{M_f(s)}{b_0}V(s) - \frac{H}{b_0}Z(s) \end{cases} \tag{27}$$

where H = [$k_p k_1 k_2$ 1], and $M_f(s) = s^3 + k_2 s^2 + k_1 s + k_p$. The output of the control system can be rewritten as:

$$U(s) = \frac{M(s)}{b_0 R(s)}V(s) - \frac{N(s)}{b_0 R(s)}Y(s) \tag{28}$$

where:

$$M(s) = (s+\omega_0)^4(s+\omega_C)^3 \tag{29}$$

$$\begin{aligned} N(s) = \; & (\omega_0^4 + 12\omega_0^3\omega_c + 18\omega_0^2\omega_c^2 + 4\omega_0\omega_c^3)s^3 \\ & +(3\omega_0^4\omega_c + 12\omega_0^3\omega_c^2 + 6\omega_0^2\omega_c^3)s^3 \\ & +(3\omega_0^4\omega_c^2 + 4\omega_0^3\omega_c^3)s + \omega_0^4\omega_c^3 \end{aligned} \tag{30}$$

$$\begin{aligned} R(s) = \; & s^4 + (4\omega_0 + 3\omega_c)s^3 + (6\omega_0^2 + 3\omega_c^2 + 12\omega_0\omega_c)s^2 \\ & +(4\omega_0^3 + \omega_c^3 + 18\omega_0^2\omega_c + 12\omega_0\omega_c^2)s \end{aligned} \tag{31}$$

From Figure 4 and (28), the equivalent model of HD-LADRC in the frequency domain is shown in 6. At this time, the relationship between the output and input of the converter can be obtained:

$$Y(s) = \frac{\frac{G_{inv}(s)H_1(s)H_2(s)}{s^3L_1CL_2+s^2CL_2G_{inv}(s)Z_C+sL_1+sL_2+sG_{inv}(s)Y_cL_2+G_{inv}(s)H_2(s)}V(s)}{-\frac{s^2L_1C+sCG_{inv}(s)Z_C+G_{inv}(s)Y_c+1}{s^3L_1CL_2+s^2CL_2G_{inv}(s)Z_C+sL_1+sL_2+G_{inv}(s)H_2(s)}U_g(s)} \tag{32}$$

where $H_1(s) = \frac{M(s)}{N(s)}$, $H_2(s) = \frac{N(s)}{b_0R(s)}$.

The internal coupling of a converter and the external coupling between the multiple converters both contribute to the fluctuation of the grid-connected voltage, and it can be regarded as the total disturbance in the control scheme. Also from the analysis, the system output includes a reference signal tracking control and total disturbance compensation. The reference signal tracking control is mainly affected by the controller bandwidth $\omega_c$. And the control system can quickly track the input variables by adjusting the controller bandwidth $\omega_c$. However, the total disturbance compensation control is more sensitive to the observer bandwidth $\omega_0$, which is the main factor affecting the stability and control accuracy of the control system.

From Figure 6, the transfer function between the input and output can be obtained as follows:

$$G_{cv}(s) = \frac{Y(s)}{V(s)} = \frac{G_{inv}(s)H_1(s)H_2(s)}{s^3L_1CL_2 + s^2CL_2G_{inv}(s)Z_C + sL_1 + sL_2 + sG_{inv}(s)Y_CL_2 + G_{inv}(s)H_2(s)} \tag{33}$$

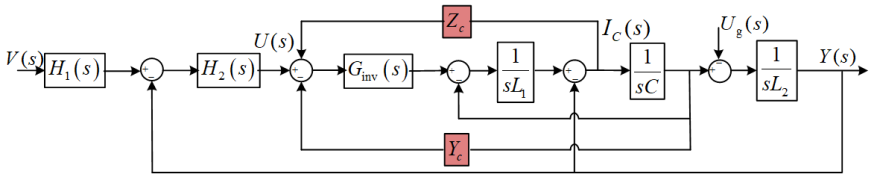


**Figure 6.** Equivalent block diagram of LCL-type converter control system in frequency domain.

In (33), the difference between the HD-LADRC and the traditional LADRC is that the molecular expression in the transfer function is different. At this time, the traditional LADRC control is the same as the analysis based on HD-LADRC control; that is, the system zero position is fixed. In the transfer function based on the HD-LADRC control, the second-order differential term of the denominator increases the capacitor current feedback coefficient, and the first-order differential term increases the capacitor voltage feedback coefficient. The system poles can be optimized by adjusting the value of the feedback coefficient. Then, the stability of system operation is improved.

Figure 7 shows the Bode diagram of the system transfer function. Figure 7a shows the influence of the controller bandwidth $\omega_c$ on the amplitude frequency characteristics of the system. It can be seen from the figure that the reference signal tracking ability is enhanced with the increase in the controller bandwidth $\omega_c$. However, the high-frequency attenuation ability is reduced. Figure 7b shows the influence of the observer bandwidth $\omega_0$ on the amplitude frequency characteristics of the system. The control gains and high frequency attenuation ability of the system hardly change with the bandwidth of the observer. However, a larger observer bandwidth $\omega_0$ will cause output noise.

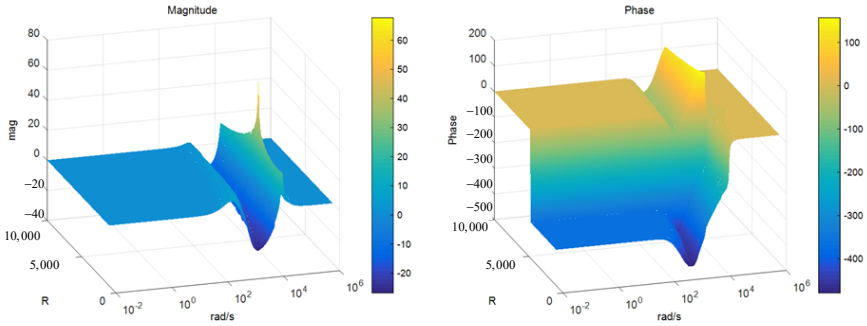


(**a**) $\omega_c$ on the amplitude frequency characteristics

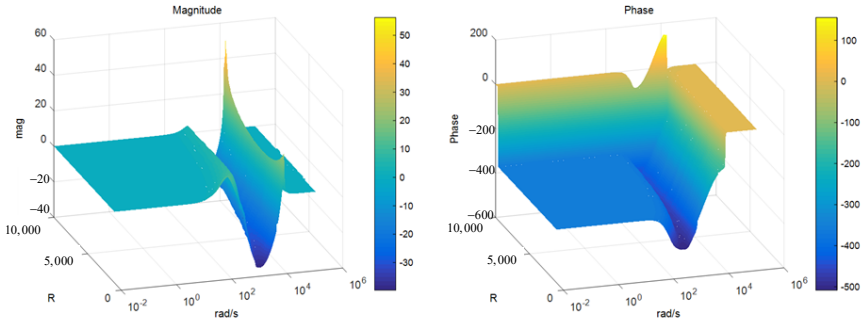


(**b**) $\omega_0$ on the amplitude frequency characteristics

**Figure 7.** Bode diagram of reference signal tracking system.

## 5. Simulation and Experimental Verification

A simulation model of three LCL-type converters operating in parallel is built in Matlab/Simulink for verification. Three operating cases are studied to verify the internal decoupling in a single converter, decoupling among parallel converters, and anti-disturbance performance of the proposed control, respectively. The proposed control strategy is verified by two 30 kW converter prototypes. The AC and DC interfaces of the converter are connected to the DC and AC power sources, respectively. The insulated gate bipolar transistor (IGBT) modules from Infineon (FF225R17ME4) are used. Table 2 shows the detailed parameters. Transient and steady-state experiments are carried out to verify the effectiveness of the proposed control method. The oscilloscope from Teledyne Lecroy is used to measure the waveforms. The hardware tests setup diagram with two paralleled converters at the same power rating is shown in Figure 8.

**Table 2.** Parameters of simulation and experimental setup.

| Parameters | Value |
|---|---|
| DC-Link | 800 V |
| $L_1$, $L_2$ | 3 mH, 1 mH |
| $C_f$ | 15 μF |
| DC Capacitor | 1100 μF |
| AC Source Voltage | 220 V |
| Switching Frequency | 10 kHz |
| $\xi$ | 0.707 |
| $\omega_c$ | 4500 |
| $\omega_0$ | 9000 |

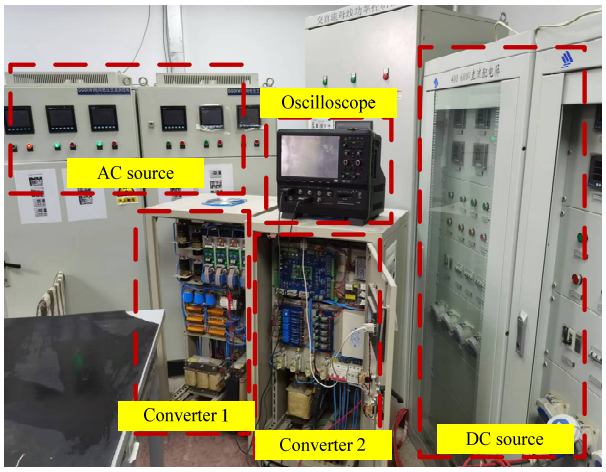


**Figure 8.** Studied system and hardware tests setup.

Case 1: Comparative analysis of the internal decoupling in a single converter.

Figure 9 shows the *dq* axis components of the output current of a single converter using conventional PI in comparison with the proposed control. Upon the active power load switching at 0.5 s, the output currents $i_d$ under both control schemes have similar transients, roughly dropping from 4 A to 1 A. In the meantime, the PI control stabilizes $i_q$ at around 2.7 A and fluctuates by 1.64 A at most. In contrast, the proposed HD-LADRC has a much lower $i_q$ that stabilizes at about 1.2 A, and the largest fluctuation is around 1.39 A. It is obvious that better decoupling between *dq* components can be attained using proposed HD-LADRC where lower $i_q$ and less fluctuations are observed.

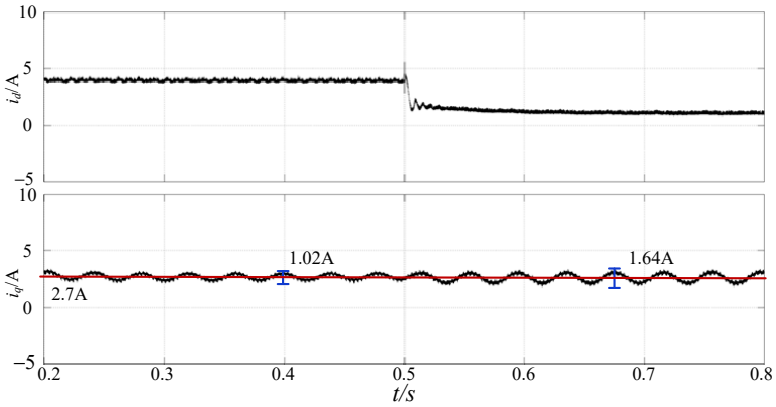


(**a**) *dq* axis components of output current using conventional PI control

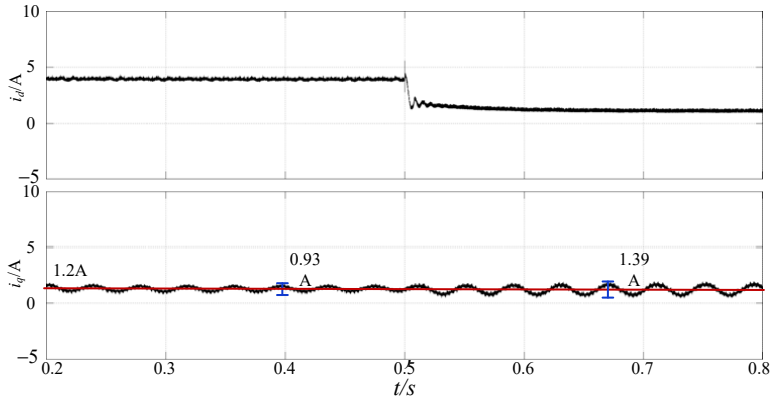


(**b**) *dq* axis components of output current using proposed control

**Figure 9.** Internal coupling suppression effects of the converter control system.

Case 2: Comparative analysis of the internal decoupling in a single converter.

Figure 10 compares the Total Harmonic Distortions (THD) of the output current of a converter working in parallel with another converter using either PI or HD-LADRC. The PI gives a THD of 5.33% which is reduced to 4.66% employing the HD-LADRC, indicating an improved decoupling between among the converters working in parallel by the proposed control scheme.

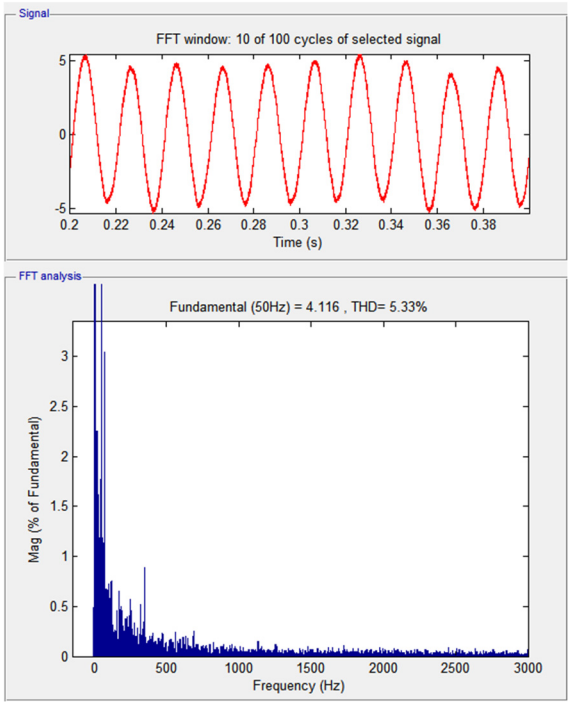


(**a**) THD of output current using PI control

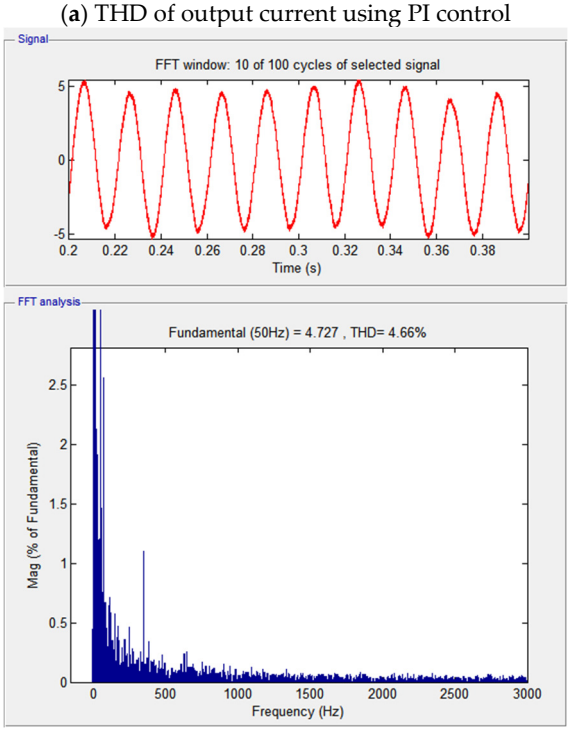


(**b**) THD of output current using the proposed control

**Figure 10.** Coupling suppression effect among multi-converters.

Experimental waveforms are given in Figure 11, where, clearly, the output current under PI control contains more distortions compared to the current when using HD-LADRC. This suggests that the output current is more effectively suppressed with HD-LADRC.

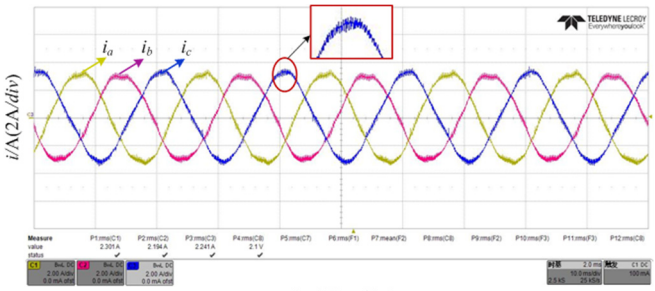


(**a**) output current using PI control

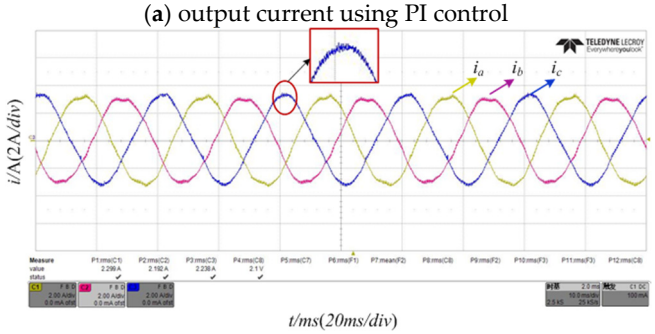


(**b**) output current using HD-LADRC control

**Figure 11.** Experimental waveforms of output currents of parallel LCL-type converters under steady-state operation.

Figure 12 compares the output current of parallel converters using different control schemes under load-switching operations. It can be seen that at 0.5 s, when load switching occurs, the output current fluctuates greatly and takes about one cycle to reaches the steady state when using PI control. In contrast, when the proposed HD-LADRC control is adopted, the response is faster and the output current fluctuates less upon the disturbance. Therefore, the proposed control offers better reference signal tracking, faster responses, and thus improved system anti-disturbance performance.

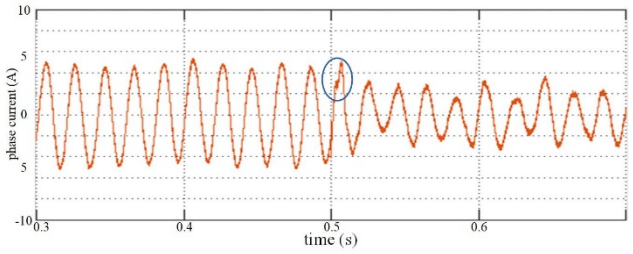


(**a**) phase current using PI control

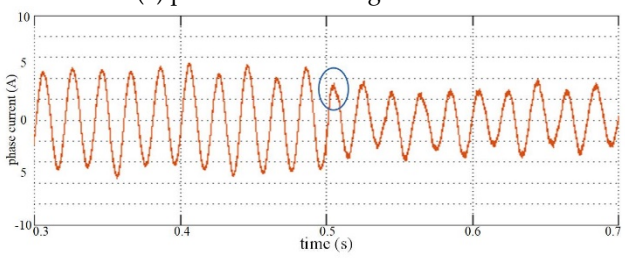


(**b**) phase current using the proposed control

**Figure 12.** Comparison and verification of anti-disturbance performance.

Case 3: Comparative analysis of anti-disturbance performance in parallel converter system.

Experimental results are given in Figure 13, where output currents using different control strategies during transient load switching are compared. Both have good anti-disturbance performance, and the steady state is reached again within 5 ms. By observing the results more closely, the transient response under HD-LADRC is less fluctuating, and the anti-disturbance performance is improved. Furthermore, the power transmission efficiency of converters is increased to a certain extent under HD-LADRC control framework.

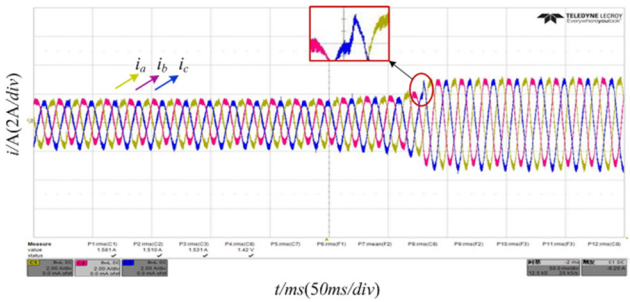


(**a**) experimental waveform of output current using PI control during load switching

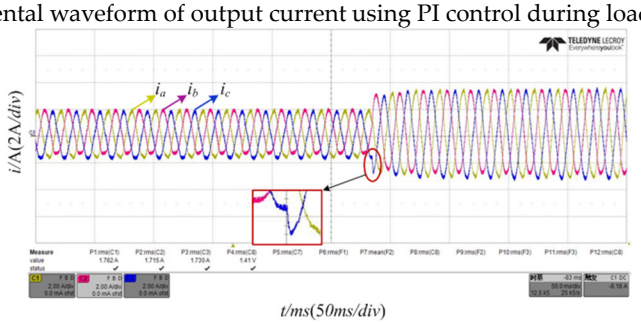


(**b**) experimental waveform of output current using HD-LADRC control during load switching

**Figure 13.** Experimental waveforms diagram of parallel LCL-type converters under load switch.

## 6. Discussion

The LCL-type converters operating in parallel will have an additional offset resonance peak on the bases of the inherent resonance peak due to internal and external disturbances such as modeling errors, the number of parallel converters, grid impedance, and control parameter differences. Traditional virtual damping control will have difficulty meeting the parallel resonance suppression requirements. This paper proposes a parallel resonance suppression method based on hybrid damping active disturbance rejection control. The superior performance of active disturbance rejection control, which can balance system overshoot and response time, has been verified by comparing the performance of active disturbance rejection control and traditional PID control. However, due to the large number and complex tuning of control parameters, linearization analysis was conducted on the active disturbance rejection control to optimize the parameter tuning method. On the basis of analyzing the state space model of LCL-type converters and combining with the relevant principles of linear self-disturbance rejection control, a current inner-loop controller based on third-order linear active disturbance rejection control is designed. The multi-dimensional coupling generated by the number of parallel units, grid impedance, parameter perturbation, etc. in the parallel converter system is classified as the total system disturbance and compensated, which will reduce the offset of the resonant point and reduce the coupling degree of the parallel converter system. A hybrid damping control method is designed to reduce the occurrence of overvoltage, overcurrent, and other situations. This control mainly includes capacitor current feedback control to suppress system resonance peaks and capacitor voltage feedback control to reduce the resonance frequency offset. In addition, the controller parameter tuning method is optimized to improve control robustness by analyzing the anti-interference ability of the converter control system. Finally, the feasibility and effectiveness of the proposed control method were verified through

simulation and experimental analysis. The Total Harmonic Distortions (THD) of the output current of a converter working in parallel with another converter using either PI or HD-LADRC is compared. The PI gives a THD of 5.33% which is reduced to 4.66% when employing the HD-LADRC. Compared with the research results of existing reference literature, Table 3 gives the THD data under different control methods, where Method I employs a conventional LCL filter. Method II adopts an ILCL filter without HD-LADRC control [7]. Method III uses a CLCL filter with an LFZSCC controller [11]. Method IV is the proposed HD-LADRC resonance suppression scheme. Table 3 gives the THD parameters under different control methods, which indicate an improved decoupling between among the converters working in parallel by the proposed control scheme. By observing the results more closely, the transient response under HD-LADRC is less fluctuating, and the anti-disturbance performance is improved. Furthermore, the power transmission efficiency of converters is increased to a certain extent under the HD-LADRC control framework. The research results indicate that the hybrid damping active disturbance rejection control proposed in this paper has better reference signal tracking and disturbance rejection performance compared to traditional PI control, which can effectively reduce the coupling between parallel converters and reduce the risk of parallel resonance induction.

**Table 3.** THD of grid side current with different methods.

| Methods | THD Value |
|---|---|
| Method—I | 5.33% |
| Method—II | 12.88% |
| Method—III | 9.56% |
| Method—IV | 4.66% |

## 7. Conclusions

In this paper, an HD-ADRC method is proposed to suppress the harmonic resonance of parallel LCL-type converters, where both the internal and external disturbances are lumped as total disturbances. A third-order linear disturbance rejection controller (LADRC) with a linear extended-state observer and an error feedback control rate is designed based on LCL-type converter model analysis. A hybrid damping control is proposed to reconstruct the damping characteristics of converters to suppress the parallel resonance spike and to reduce the resonance frequency offset. The parameter selection of the control system is optimized through the stability analysis of tracking performance and anti-disturbance performance of the HD-ADRC controller. The simulation and experimental results show that the PI controller gives a THD of 5.33%, which is reduced to 4.66% when employing the HD-LADRC, indicating an improved decoupling between among the converters working in parallel by the proposed control scheme. The HD-LADRC control strategy proposed in this paper has a good decoupling ability for the parallel converter. However, the third-order control scheme will lead to a calculation time extension, which will affect the dynamic performance of the control system. In the follow-up study, we will focus on the reduction of the order operation of the LADRC control strategy to improve the response ability of the control system and the difficulty of parameter tuning.

**Author Contributions:** M.Q.: methodology, software, validation, investigation, data curation, writing—original draft preparation; B.Z.: methodology, software, validation, investigation, writing—review and editing, project administration, software; J.Z.: writing—review and editing, data curation; W.Q.: writing—review and editing, software; N.C.: writing—review and editing; Y.L.: writing—review and editing. All authors have read and agreed to the published version of the manuscript.

**Funding:** This research was funded by the Key R&D Program of Shanxi Province-202304290000007, and Fundamental Research Program of Shanxi Province-202203021212288.

**Data Availability Statement:** The original contributions presented in the study are included in the article, further inquiries can be directed to the corresponding author.

**Conflicts of Interest:** The authors declare no conflict of interest.

## Nomenclature

| **Nomenclature** | *Indices and sets* | **Nomenclature** | *Indices and sets* |
|---|---|---|---|
| $i_{1k}$ | converter side current | $U_{dc}$ | DC voltage |
| $u_{ck}$ | filter capacitor voltage | $T_s$ | sampling period |
| $i_{2k}$ | grid side current | $G_t(s)$ | Norton equivalent controlled-current source coefficient |
| $u_{1k}$ | converter output voltage | $G_t(s)i_{2ref}(s)$ | equivalent controlled-current source |
| $u_{pcc}$ | voltage of PCC | $Y_{eq}(s)$ | equivalent output admittance of the converter |
| $i_{1d}$, $i_{1q}$ | $dq$ components of converter side current $i_{1k}$ | $G_i(s)$ | transfer function of PI controller |
| $i_{2d}$, $i_{2q}$ | $dq$ components of grid side current $i_{2k}$ | $G_{LCL}(s)$ | transfer function of LCL filter |
| $u_{cd}$, $u_{cq}$ | $dq$ components of filter capacitor voltage $u_{ck}$ | $G_{inv}(s)$ | gain of the transform bridge including digital control delay |
| $Y_g(s)$ | equivalent admittance of power grid | $f_{0d}$, $f_{0q}$ | $dq$ axis components of internal disturbances including coupling components |
| $U_g(s)$ | ideal grid voltage | $w_d$, $w_q$ | $dq$ axis components of external disturbances |
| $Z_g$ | grid impedance | $\beta_1$, $\beta_2$, $\beta_3$, $\beta_4$ and $\omega_0$ | observer gains and bandwidth, respectively |
| $v$ | reference input | $u_0$ | proportional feedback controller of the system |
| $b_0$ | controller gain | $k_p$, $k_1$ and $k_2$ | controller gains |
| $u$ | control output | $\xi$ | damping coefficient |
| $y$ | system output | $f_n$ | natural frequency of the system without damping |
| $z_1$~$z_4$ | observation values of the system state variables | $b_0 = 1/(L_1CL_2)$ | approximate estimation of the system control gain |
| $Z_c$ | capacitor current feedback coefficient | $\Delta b$ | system modeling error |
| $Y_c$ | capacitor voltage feedback coefficient | $u_d$, $u_d$ | $dq$ axis components of the control system output |

## References


1. Ana, F.; Antonio Vigueras, R.; Ángel, M.G. Analysis of power system inertia estimation in high wind power plant integration scenarios. *IET Renew. Power Gener.* **2019**, *15*, 2807–2816.
2. Rakesh, K.P.; Abheejeet, M.; Suresh, C.S. Enhancing inertia of solar photovoltaic-based microgrid through notch filter-based PLL in SRF control. *IET Gener. Transm. Distrib.* **2020**, *3*, 379–388.
3. Wang, Y.; Liu, B.; Duan, S. Modified virtual inertia control method of VSG strategy with improved transient response and power-supporting capability. *IET Power Electron.* **2019**, *12*, 3178–3184. [CrossRef]
4. Zhang, B.; Han, X.; Ren, C.; Zhang, D.; Wang, L.; Song, T. Circulating Current Suppression Method with Adaptive Virtual Impedance for Multi-bidirectional Power Converters Under Unbalanced Conditions. *CSEE J. Power Energy Syst.* **2023**, *1*, 77–87.
5. Zhang, R.; Zhang, C.; Xing, X.; Chi, S.; Liu, C.; Fang, J. Modeling and Attenuation of Common Mode Resonance Current for Improved LCL-Type Parallel Inverters in PV Plants. *IEEE Trans. Ind. Inform.* **2024**, *20*, 5193–5205. [CrossRef]
6. Ruiz, G.E.M.; Muñoz, N.; Cano, J.B. Modeling, analysis and design procedure of LCL filter for grid-connected converters. In Proceedings of the 2015 IEEE Workshop on Power Electronics and Power Quality Applications (PEPQA), Bogota, Colombia, 2–4 June 2015; pp. 1–6.
7. Li, X.; Xing, X.; Qin, C.; Zhang, C.; Zhang, G. Design and Control Method to Suppress Resonance Circulating Current for Parallel Three-Level Rectifiers with Modified LCL Filter. *IEEE Trans. Ind. Electron.* **2021**, *68*, 7012–7023. [CrossRef]

8. Roldán-Pérez, J.; Bueno, E.J.; Peña-Alzola, R.; Rodríguez-Cabero, A. All-pass-filter-based active damping for VSCs with LCL filters connected to weak grids. *IEEE Trans. Power Electron.* **2018**, *11*, 9890–9901. [CrossRef]
9. Zhang, B.; Han, X.; Meng, R.; Ren, C.; Wang, L.; Song, T.; Liu, Y. Adaptive virtual impedance control based on second-order generalized integral for circulating current suppression. *J. Power Electron.* **2021**, *1*, 13–26. [CrossRef]
10. Zhang, B.; Han, X.; Jia, Y.; Meng, R.; Wang, L.; Ren, C.; Song, T. Research on Circulating Current Suppression Method of Paralleled Multi-bidirectional Power Converter Based on Unified Voltage Control. In Proceedings of the 2019 IEEE Power & Energy Society General Meeting (PESGM), Atlanta, GA, USA, 4–8 August 2019; pp. 1–5.
11. Zhang, C.; Li, X.; Xing, X.; Zhang, B.; Zhang, R.; Duan, B. Modeling and Mitigation of Resonance Current for Modified LCL-Type Parallel Inverters with Inverter-Side Current Control. *IEEE Trans. Ind. Inform.* **2022**, *18*, 932–942. [CrossRef]
12. Xia, Y.; Yu, M.; Peng, Y.; Wei, W. Modeling and Analysis of Circulating Currents Among Input-Parallel Output-Parallel Nonisolated Converters. *IEEE Trans. Power Electron.* **2018**, *10*, 412–8426. [CrossRef]
13. Dong, D.; Wen, B.; Boroyevich, D.; Mattavelli, P.; Xue, Y. Analysis of Phase-Locked Loop Low-Frequency Stability in Three-Phase Grid-Connected Power Converters Considering Impedance Interactions. *IEEE Trans. Ind. Electron.* **2015**, *1*, 310–321. [CrossRef]
14. Wu, W.; Sun, Y.; Huang, M.; Wang, X.; Wang, H.; Blaabjerg, F.; Liserre, M.; Chung, H.S.-H. A Robust Passive Damping Method for LLCL-Filter-Based Grid-Tied Inverters to Minimize the Effect of Grid Harmonic Voltages. *IEEE Trans. Power Electron.* **2014**, *7*, 3279–3289. [CrossRef]
15. Saïd-Romdhane, M.B.; Naouar, M.W.; Slama-Belkhodja, I.; Monmasson, E. Robust Active Damping Methods for LCL Filter-Based Grid-Connected Converters. *IEEE Trans. Power Electron.* **2017**, *32*, 6739–6750. [CrossRef]
16. Beres, R.N.; Wang, X.; Liserre, M.; Blaabjerg, F.; Bak, C.L. A Review of Passive Power Filters for Three-Phase Grid-Connected Voltage-Source Converters. *IEEE J. Emerg. Sel. Top. Power Electron.* **2016**, *1*, 54–69. [CrossRef]
17. Yao, W.; Yang, Y.; Zhang, X.; Blaabjerg, F.; Loh, P.C. Design and analysis of robust active damping for LCL filters using digital notch filters. *IEEE Trans. Power Electron.* **2017**, *3*, 2360–2375. [CrossRef]
18. Rathore, K.; Vakacharla, V.R. A Simple Technique for Fundamental Harmonic Approximation Analysis in Parallel and Series–Parallel Resonant Converters. *IEEE Trans. Ind. Electron.* **2020**, *67*, 9963–9968. [CrossRef]
19. Zeng, C.; Wang, H.; Li, S.; Miao, H. Grid-Voltage-Feedback Active Damping with Lead Compensation for LCL-Type Inverter Connected to Weak Grid. *IEEE Access* **2021**, *9*, 106813–106823. [CrossRef]
20. He, Y.; Wang, X.; Ruan, X.; Pan, D.; Qin, K. Hybrid Active Damping Combining Capacitor Current Feedback and Point of Common Coupling Voltage Feedforward for LCL-Type Grid-Connected Inverter. *IEEE Trans. Power Electron.* **2021**, *36*, 2373–2383. [CrossRef]
21. Zhou, J.; Yao, Y.; Huang, Y.; Peng, F. Motor Current Feedback-Only Active Damping Controller with High Robustness for LCL-Equipped High-Speed PMSM. *IEEE Trans. Power Electron.* **2023**, *38*, 8707–8718. [CrossRef]
22. Liu, J.; Sun, X.; Chen, Z.; Chi, Y.; Song, W.; Zhu, Q.; Wheeler, P. A Hybrid Multiresonances Suppression Method for Non-synchronous LCL-Type Grid-Connected Inverter Clusters Under Weak Grid. *IEEE Trans. Power Electron.* **2024**, *39*, 5386–5399. [CrossRef]
23. Ma, W.; Guan, Y.; Zhang, B.; Wu, L. Active Disturbance Rejection Control Based Single Current Feedback Resonance Damping Strategy for LCL-Type Grid-Connected Inverter. *IEEE Trans. Energy Convers.* **2021**, *36*, 48–62. [CrossRef]
24. Li, Y.; He, J.; Liu, Y.; Ren, Y.; Li, Y.W. Decoupled Mitigation Control of Series Resonance and Harmonic Load Current for HAPFs with a Modified Two-Step Virtual Impedance Shaping. *IEEE Trans. Ind. Electron.* **2023**, *70*, 8064–8074. [CrossRef]
25. Liu, Q.; Liu, F.; Zou, R.; Li, Y. Harmonic Resonance Characteristic of Large-Scale PV Plant: Modelling, Analysis, and Engineering Case. *IEEE Trans. Power Deliv.* **2022**, *37*, 2359–2368. [CrossRef]
26. Shen, H.; Liu, Z.; Liu, W.; Wang, C.; Sun, X.; Yang, F.; Zhang, M. High Frequency Resonance Analysis and Resonance Suppression of a Grid-Connected Inverter Coupled with a Long Feeder. *IEEE Trans. Power Deliv.* **2023**, *38*, 926–936. [CrossRef]
27. Ji, K.; Yang, Y. Harmonic Power Detection-Based Adaptive Resonance Suppression for Power Converters. *IEEE Trans. Power Deliv.* **2024**, *39*, 601–612. [CrossRef]
28. Gao, Z. Scaling and bandwidth-parameterization based controller tuning. In Proceedings of the 2003 American Control Conference, Denver, CO, USA, 4–6 June 2003; Volume 6, pp. 4989–4996.
29. Ouyang, Q.; Fan, K.; Liu, Y.; Li, N. Adaptive LADRC Parameter Optimization in Magnetic Levitation. *IEEE Access* **2021**, *9*, 36791–36801. [CrossRef]
30. Xie, Z.; Chen, Y.; Wu, W.; Gong, W.; Zhou, L.; Zhou, X.; Guerrero, J.M. Admittance Modeling and Stability Analysis of Grid-Connected Inverter with LADRC-PLL. *IEEE Trans. Ind. Electron.* **2021**, *12*, 12272–12284. [CrossRef]
31. Guo, C.; Li, H.; Wang, Z.; Hou, Y. Research on Compensation of Three-Phase Unbalanced Voltage of Microgrid Based on LADRC. In Proceedings of the 2020 5th International Conference on Power and Renewable Energy (ICPRE), Shanghai, China, 12–14 September 2020; pp. 424–428.
32. Benrabah, A.; Xu, D.; Gao, Z. Active Disturbance Rejection Control of LCL-Filtered Grid-Connected Inverter Using Padé Approximation. *IEEE Trans. Ind. Appl.* **2018**, *6*, 6179–6189. [CrossRef]
33. He, H.; Si, T.; Sun, L.; Liu, B.; Li, Z. Linear Active Disturbance Rejection Control for Three-Phase Voltage-Source PWM Rectifier. *IEEE Access* **2020**, *8*, 45050–45060. [CrossRef]
34. Zhou, X.; Cui, Y.; Ma, Y. Fuzzy Linear Active Disturbance Rejection Control of Injection Hybrid Active Power Filter for Medium and High Voltage Distribution Network. *IEEE Access* **2021**, *9*, 8421–8432. [CrossRef]

35. Wu, Y.; Xu, J.; Ling, Z.; Qian, H.; Xie, S. Full-Order State Observer Based Control for LCL-Filtered Grid-Connected Inverter with Only One Current Sensor. In Proceedings of the 2021 IEEE 16th Conference on Industrial Electronics and Applications (ICIEA), Chengdu, China, 1–4 August 2021; pp. 965–970.
36. Yang, D.; Wang, X.; Blaabjerg, F. Investigation of the sideband effect for the LCL-type grid-connected inverter with high LCL resonance frequency. In Proceedings of the 2017 IEEE Energy Conversion Congress and Exposition (ECCE), Cincinnati, OH, USA, 1–5 October 2017; pp. 5601–5606.
37. Wang, S.; Zhu, H.; Wu, M.; Zhang, W. Active Disturbance Rejection Decoupling Control for Three-Degree-of- Freedom Six-Pole Active Magnetic Bearing Based on BP Neural Network. *IEEE Trans. Appl. Supercond.* **2020**, *30*, 1–5. [CrossRef]
38. Carreño-Zagarra, J.J.; Moreno, J.C.; Guzmán, J.L. Optimal Active Disturbance Rejection Control for Second Order Systems. *IEEE Access* **2024**, *12*, 76244–76256. [CrossRef]
39. Li, M.; Wu, Z.-H.; Deng, F.; Guo, B.-Z. Active Disturbance Rejection Control to Consensus of Second-Order Stochastic Multiagent Systems. *IEEE Trans. Control Netw. Syst.* **2023**, *10*, 993–1004. [CrossRef]
40. Zou, S.; Zhao, W.; Wang, C.; Liang, W.; Chen, F. Tracking and Synchronization Control Strategy of Vehicle Dual-Motor Steer-by-Wire System via Active Disturbance Rejection Control. *IEEE/ASME Trans. Mechatron.* **2023**, *28*, 92–103. [CrossRef]